Electronic Supplementary Material (ESI) for Nanoscale.

Supporting Information

Atomic scale reversible opto-structural switching of few atom luminescent silver clusters confined in LTA zeolites

Saleh Aghakhani,[a] Didier Grandjean,*[a] Wouter Baekelant,[b] Eduardo Coutiño-Gonzalez,[b,c] Eduard Fron,[b] Kristina Kvashnina,[d,e] Maarten B. J. Roeffaers,[f] Johan Hofkens,[b] Bert F. Sels,[f] and Peter Lievens[a]

[a]Department of Physics and Astronomy, Laboratory of Solid State Physics and Magnetism, KU Leuven, Celestijnenlaan 200D, 3001 Leuven, Belgium. [b]Leuven Chem &Tech: Molecular Imaging and Photonics (MIP), KU Leuven, Celestijnenlaan 200F, 3001 Leuven, Belgium. [c]CONACYT - Centro de Investigación y Desarrollo Tecnológico en Electroquímica, Parque Industrial Querétaro, Sanfandila s/n, Pedro Escobedo 76703, Querétaro, Mexico. [d] Rossendorf Beamline at ESRF-The European Synchrotron, CS40220, 38043 Grenoble Cedex 9, France. [e]Helmholtz Zentrum Dresden-Rossendorf (HZDR), Institute of Resource Ecology, PO Box 510119, 01314 Dresden, Germany. [f]DUBBLE CRG-ESRF- The European Synchrotron, CS 40220, 38043 Grenoble Cedex 9, France. [g]Leuven Chem &Tech: Centre for Surface Chemistry and Catalysis (COK), KU Leuven, Celestijnenlaan 200F, 3001 Leuven, Belgium.

Content

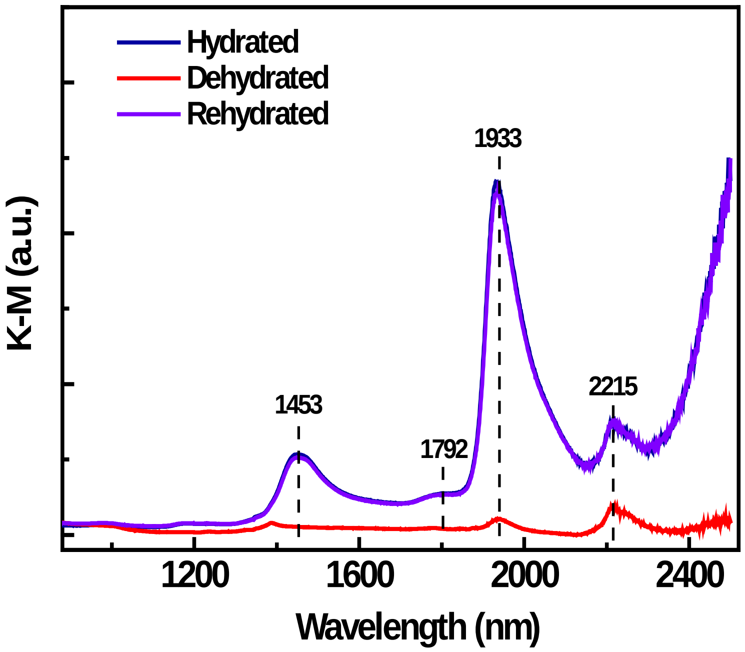

Figure S1. NIR DRS spectra of sample in different hydration states.

NIR DRS Spectroscopy Analysis

Figure S1 presents the assignment of the overtone and combination vibrational bands of water and hydroxyls in the sodalite in the NIR range. These attenuated bands are complementary to the FTIR results for the identification of the different water and hydroxyl types appearing in the material according to the water content. Three important NIR bands can be assigned as follows: A). Overtone of the hydroxyl vibration [(2*ν_S OH)] at 1450-1475 nm (depending on the type of OH group), B). Combination of the water and hydroxyl vibration [(ν_S + ν_δ) H_2O] at 1900-1950 nm (depending on the type of zeolitic water and its interaction with the (non)-framework atoms), and C). Combination of symmetric and bending vibration of Si-O(H)-Al [(ν_S + ν_δ) Si-O(H)-Al] around 2215 nm.[1] These bands appear only in the presence of water, except the band at 2215 nm, which remains almost constant upon dehydration. This might be related to the major contribution of structural Si-O-Al vibrations in the absence of significant hydroxyls.

XAFS Spectroscopy Analysis

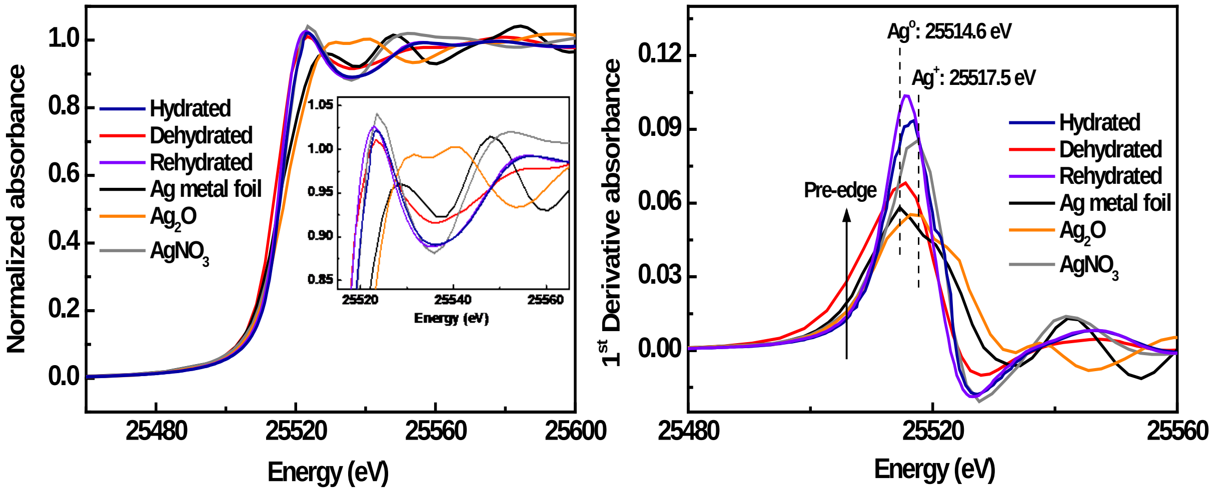

Figure S2. Ag K-edge A). Normalized and B). First derivative XANES spectra of a Ag_3Na_9LTA sample in different hydration states compared to Ag metal foil (Ag°), Ag_2O (Ag^+), and $AgNO_3$ (Ag^+) reference. The Ag edge position of references are indicated in profile B for better clarification of the sample charge in each hydration state.

XANES

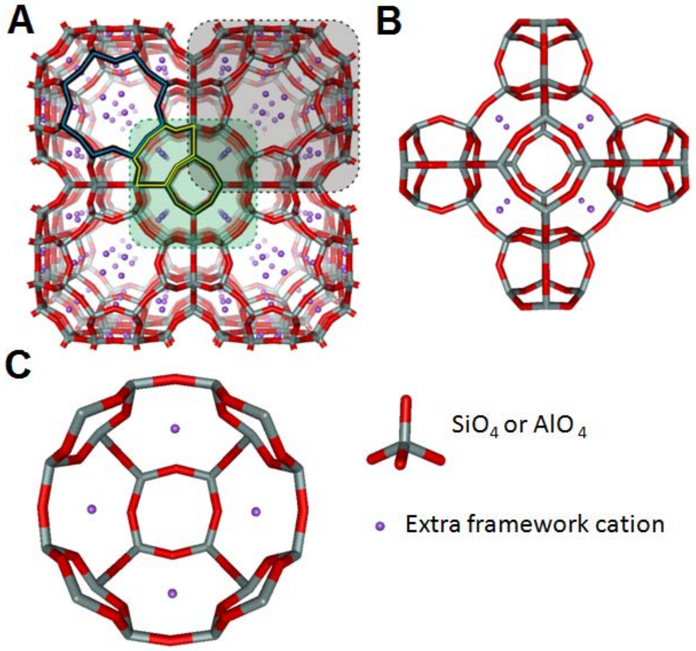

Figure S3. Schematic representation of A) LTA unit cell displaying the sodalite (green dashed area) and super cage (gray dashed area); the eight ring (8R), single six ring (S6Rs), and double four rings (D4Rs) are highlighted in blue, yellow and green respectively, B) Isolated sodalite cage with D4R connectors, and C) Transversal section of a sodalite cage.

LTA Zeolite Unite Cell

EXAFS

Details of the EXAFS fitting parameters are given in Table S1. Based on AgCLs in LTA crystallographic data[2-4] and clarify better the nature of Ag atoms, two distinct geometrical positions are taken into account: I). Ag atoms forming AgCLs (Ag_c) located inside the sodalite and II). Ag cations occupying the sodalite S6Rs (Ag_{6R}). Ag_c and Ag_{6R} fractions are then required to calculate the coordination number (CN_i) of each shell. The Ag_{6R} fraction is obtained from the Ag_{6R} CN with the $(Si/Al)_{6R}$ divided by six ($CN_5/6$, Table S1) as the maximum CN to Si or Al atoms in the S6Rs. Then, The Ag_C fraction is simply derived by considering that $Ag_c+Ag_{6R}=1$. These fractions are tabulated in Table S1.

Table S1. Summary of Ag-K edge EXAFS structural refinements of samples with different hydration state.

		Hydrated			Dehydrated			Rehydrated		
N_i	**Shell**	**CN_i**	**R_i(Å)**	**A_i(Å^2)**	**CN_i**	**R_i(Å)**	**A_i(Å^2)**	**CN_i**	**R_i(Å)**	**A_i(Å^2)**
1	**Ag_{C+6R}-O**	2.6(5)	2.33(2)	0.025(3)	1.8(3)	2.27(1)	0.018(2)	2.6(2)	2.33(2)	0.024(2)
2	**Ag_c-Ag_c**	2.0(4)	2.72(3)	0.041(3)	1.5(3)	2.75(6)	0.072(6)	1.9(4)	2.73(2)	0.040(3)
3	**Ag_c-O**	0.4(2)	3.17(2)	0.038(4)	0.9(2)	2.81(4)	0.035(4)	0.4(2)	3.18(1)	0.035(3)
4	**Ag_{6R}-(Si/Al)**	2.0(4)	3.29(2)	0.018(2)	3.7(6)	3.25(1)	0.024(4)	2.1(4)	3.27(2)	0.016(2)
5	**Ag_c -Na**	0.5(3)	3.24(3)	0.015(2)	0.5(2)	3.01(3)	0.025(3)	0.3(1)	3.19(3)	0.008(1)
6	**Ag_c-Ag_{6R}**	0.4(2)	3.42(2)	0.023(3)	0.6(2)	3.40(3)	0.021(2)	1.2(3)	3.41(2)	0.033(2)
		Ag_c:Ag_{6R} 66%:34%		R*=19.50%	Ag_c:Ag_{6R} 38%:62%		R*=23.76%	Ag_c:Ag_{6R} 65%:35%		R*=16.76%

N_i: Shell number, **CN_i:** Coordination number of atom in the N_i^{th} shell, **R_i:** Radial distance of atoms in the N_i^{th} shell [Å], **A_i**: Debye-Waller term of the N_i^{th} shell ($A=2\sigma^2$ with σ^2= Debye-Waller factor)[Å^2], **R*:** Error factor (%) **Ag_C**: Ag atom composed of AgCLs, **Ag_{6R}**: Ag cation coordinated with the six memberd ring, **Ag_c:Ag_{6R}** percentage of the Ag_c and the Ag_{6R} in each EXAFS model.

Fitting the data with a six-shell model (Table S1) showed a good agreement with the 3D crystallographic model of LTA sodalite cage. Hydrated and rehydrated samples could be fitted with a very similar model consisting of a first shell (N_1) corresponding in both states to 2.6 O located at 2.33 Å. This shell corresponds to a mixture of single cations Ag_{6R} located on the axis of the S6Rs of the sodalite cage coordinated to framework O_{6R} and Ag_c forming clusters that are coordinated to extra-framework water (O_w). Furthermore, the Ag_{6R}-O_{6R} distance is shorter than the sum of Ag^+ and O^{2-} radii (2.58 Å)[2] which is attributed to the covalent bond nature of the Ag_{6R}-O_{6R} bond. Ag_{6R} are also coordinated to Si/Al atoms from the S6Rs at a distance of 3.27-3.29 Å forming shell (N_4). As Ag_{6R} are coordinated to 6 Si/Al and 3 O implying a 2:1 CN ratio[2, 3], CN_4 can be used to determine both Ag_{6R}/Ag_C and the O_w/O_{6R} ratio. CN_4 of 2 and 2.1 in hydrated and rehydrated sample, respectively, indicate a similar Ag_{6R} fraction of 34% (2.1/6*100) with the remaining part of 66% forming clusters Ag_C. As Ag_{6R} in S6Rs are coordinated to 3.0 O_{6R} [0.34*3=1] 1 O from shell N1 is an O_{6R} while the remaining 1.6 O (CN_1-1.0) is attributed to O_w of water molecules that are coordinated with the Ag_c in the sodalite with an average CN of Ag_c-O_w:2.4 [(CN_1-1.0)/0.66]. To extract the average Ag_c-O_w distance from the R_1, the average Ag_{6R}-O_{6R} and Ag_{6R}-$(Si/Al)_{6R}$ distances of 2.30 and 3.28 Å respectively were considered based on the crystallographic data of Ag_{12}LTA.[3] Thus, the Ag_c-O_w distance of 2.36 Å can be simply derived by considering the contribution of Ag_{6R}-O_{6R} and Ag_c-O_w sub-shell in the first shell [(2.6*2.33)=(1.6***2.36**)+(1.0*2.30)]. This estimated distance is in good agreement with reported XRD data (2.40 Å).[4]

The second shell (N_2) consists of intracluster Ag_c-Ag_c interactions with distances of 2.72 and 2.73 Å in the hydrated and rehydrated state respectively that are considerably shorter than typical Ag-Ag in Ag metal (2.89 Å).[4] Ag_c are coordinated with ca. 3.0 other Ag_c (CN_2/0.66) forming tetrahedral Ag_4 clusters. The average CN Ag_c-O_w of 2.4 suggests a mixture of ca. 80% [$2.4O_w/(2.4O_w+0.6O_{6R})$] tetrahedral [$Ag_4(H_2O)_4$] and 20% (1-0.8) tetrahedral [$Ag_4(O_{6R})_2$] clusters.

The third shell (N_3) with larger distance (3.17 Å, R_3) is related to the direct interaction of Ag_c with the framework oxygen (O_F) when water molecules are locally absent around the clusters. The large Ag_c-O_F distance (3.17-3.18 Å, R_3) and small CN (0.6, CN_3/0.65) in the hydrated material can be found when tetrahedral Ag_4 clusters are oriented along the S6Rs axis and partially interacting with the O_{6R} (CN_3 compared to CN_1). In this state, local dehydration induced by the X-Ray beam may explain the presence of this shell that was also observed in previous EXAFS studies.[5, 6]

N_5 and N_6 correspond to the long interaction between Ag_C from the clusters and the cations located in the axis of the S6Rs of the sodalite cage. The Ag_c-Na shell (N_5) is attributed to the interaction of Ag_c with Na co-cation residing on the axis of the S6Rs with a distance of 3.01-3.24 Å (R_4), and CN_5 0.3-05 in the hydrated and rehydrated states respectively. In this structural configuration, a Na-O_F distance of 2.41-2.50 Å can be derived which is higher than the sum of Na^+ and O^{-2} radii (2.29 Å)[2] and corresponds to an electrostatic interaction with O_{6R} unlike Ag_{6R}-O_{6R} bond in the S6Rs that possesses a covalent character. Finally shell (N_6) is assigned to long range (3.40-3.42 Å, R_6) interaction of the Ag_c with the Ag_{6R}. The significant increase of Ag_c-Ag_{6R} CN_6 (0.3-1.2) through rehydration probably indicates a redistribution of Ag and Na cations in the S6Rs around the clusters with a higher occupancy of the empty S6Rs by Ag_{6R} at the expense of Na cations whose coordination decreases from 0.5 to 0.3 in the rehydrated state. This is the only observed significant structural difference between the hydrated and rehydrated state.

Although the fitting model for the dehydrated state is very similar to the one used in the hydrated states marked differences appear. The first difference is observed in CN_1 of the first O shell that significantly decreases from 2.6 in the (re)hydrated states to 1.8 in the dehydrated sample while the Ag-O bond distance shortens from 2.30 to 2.27 Å reflecting the loss of water molecules around Ag_C atoms.

The second difference is a significant decrease in N_3 shell Ag_c-O_F distance from 3.18 to 2.81 Å, R_3 while CN_3 remarkably increases to 2.4 (0.9/0.38). This Ag_c-O_F distance corresponds to Ag_C atoms located on the axis of the S4Rs inside the sodalite cage that are now strongly interacting with O_{4R} atoms indicating that the position of the AgCLs relative to the sodalite cage has completely changed upon dehydration.

The large increase of CN_4 of the Si/Al atoms shell from 2 in the (re)hydrated states to 3.7 indicates that a larger fraction of Ag_R are now positioned on the axis of S6Rs corresponding to a larger Ag_R fraction (3.7/6*100) 62% in the material. The fact that N_1 is exactly half the value of N_4 confirms that all the O in N_1 consist of O_{6R} and no water molecule are now present around the Ag_c.

Finally, the different values observed for the N_2 shell corresponding to the Ag_C-Ag_C interaction in the clusters with a lower CN_2 of 1.5 and a larger Ag_C-Ag_C distance of 2.75 Å are clearly an indication of the formation of larger AgCLs with an average coordination of 4 (CN_2/0.38) corresponding to Ag_6 clusters upon dehydration. These values are compatible with the transformation of tetrahedral Ag_4 clusters coordinated to water molecules and located along S6Rs axis into octahedral Ag_6 clusters positioned along the S4Rs axis and coordinated only to O_{4R} atoms. The simulteous increase of AgCLs size and distance are in line with similar dehydrated AgCLs structures in Ag LTA that were identified by XRD[4, 7] and ESR.[8] No major changes upon dehydration are observed for shells N_5 and N_6 corresponding to the long interaction between Ag_C from the clusters and the cations located along the axis of the S6Rs of the sodalite cage.

FTIR Analysis

FTIR spectra of the Ag_3Na_9LTA zeolite in the mid-IR region (4000-500 cm^{-1}, Figure S4A) are composed of the framework vibrational (T-O-T; T: Si, Al), the water (ν_δ HOH), and the hydroxyl (ν_s OH) bands appearing in the spectral region of 1400-500, 1700-1600, and 3700-2900 cm^{-1}, respectively. The T-O-T vibrations are divided into three main IR bands: the asymmetric vibrations of bridge bonds [ν_{as} Si-O-Si (Al)] at 1006 cm^{-1}, the symmetric vibrations of bridge bonds [ν_s Si-O-Si (Al)], and C) at 726 and 670 cm^{-1} and the symmetric stretching of vibrational bands formed by superposition of the 4Rs 6Rs, and D4Rs[9-11] appearing at 555 cm^{-1} .

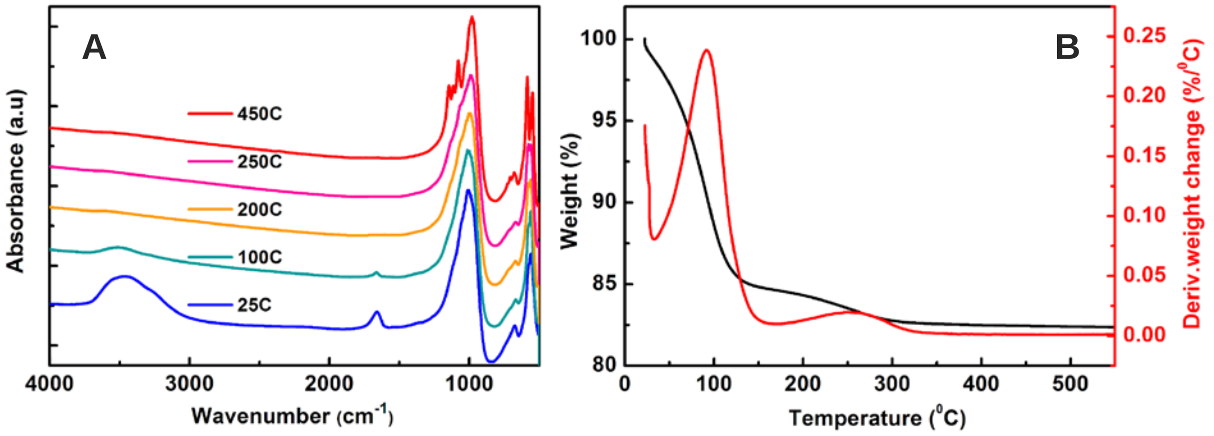

Figure S4. A). In-situ FTIR spectra of sample dehydrated in vacuum at different temperature B). TGA analysis of sample in nitrogen gas atmosphere.

The dehydration behaviour of Ag_3Na_9LTA was characterized both by FTIR and TGA analysis (Figure S4). According to the TGA result, most of the water is removed by dehydration at 100 °C (~ 83%) while the remaining part is only eliminated at higher temperatures (330 °C). FTIR results show that the intensity of ν_δ HOH and ν_s OH significantly decreases up to 100 °C (~ 75%, in line with TGA results) and completely flattens out at 200 °C. The dehydration rate is clearly faster in vacuum (FTIR) than in atmospheric nitrogen gas (TGA). T-O-T bands remain considerably unaltered in this temperature range. The emergence of new bands in this region is observed upon further dehydration above 200 °C. These bands become more pronounced when the dehydration temperature reaches 450 °C (dehydrated state). In parallel, the T-O-T bands are shifted, reaching the maximum band shift.

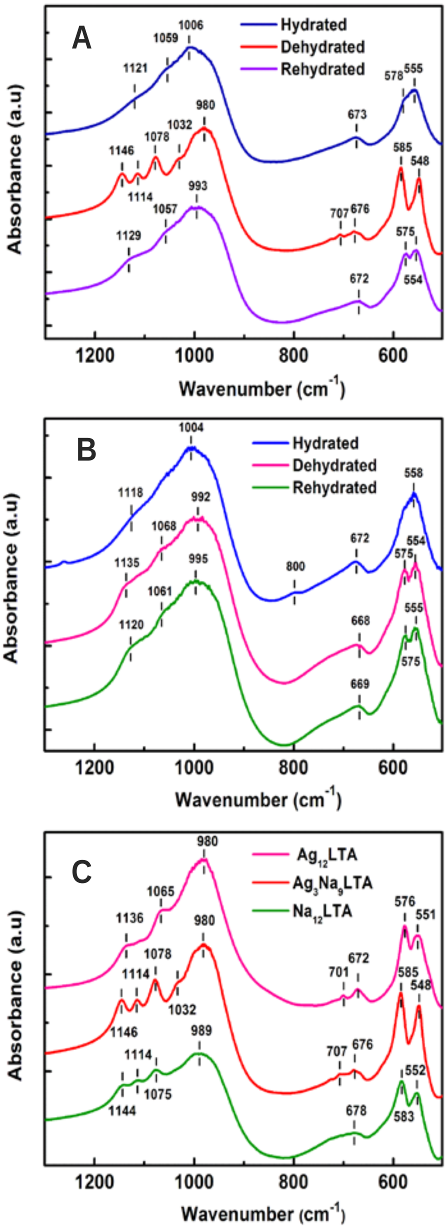

Figure S5. FTIR spectra of Ag_3Na_9LTA sample in different hydration states to monitor T-O-T (T=Si/Al) vibrational bands in A). Vacuum and B). Atmospheric oxygen gas condition. C). FTIR spectra of Ag_3Na_9LTA sample compared to parent LTA ($Na_{12}LTA$) and fully loaded Ag LTA ($Ag_{12}LTA$) zeolite in dehydrated state where the T-O-T distortion and shifted bands are at maximum.

The nature of these perturbations and band shifts (within 1200-900 cm^{-1}) has been ascribed to the coordination of metal cations with the zeolite O_F and the local electronic redistribution of the cationic sites, leading to a weakening of the T-O framework bonds, an elongation of the T-O distances, and a change of the T-O-T angles.[12-14] Therefore, these results suggest that the loss of coordinated water from the cationic sphere of Ag and Na induces their stronger interaction and higher coordination degree with the O_F which cause in turn T-O-T distortions and larger band shifts.[15, 16]

T-O-T bands clearly observed through dehydration (Figure S5 A) intensify when reaching the fully dehydrated state (450 °C). Upon dehydration a stronger T-O-T distortion, new T-O-T bands formation, and larger T-O-T band shifts due to the higher interaction degree of the Ag and Na cations with the O_F are observed. These distorted and shifted bands are not remarkable in an oxygen (Figure S5 B) environment, suggesting that these changes originate from the loss of coordinated water ligands and the lack of replaceable ligands. These bands relax upon rehydration due to the re-coordination of Ag and Na cations with water whose strong electron donation weakens the cation interaction with O_F.[15, 17, 18] To assign separately the distorted and shifted T-O-T bands to specific location and interaction type with the AgCLs, Na, and Ag cations, the T-O-T vibrations of the Ag_3Na_9LTA sample are compared with parent LTA ($Na_{12}LTA$) and fully loaded Ag LTA ($Ag_{12}LTA$)[19] in the dehydrated state (Figure S5 C). The distorted and shifted bands are less intense in $Ag_{12}LTA$ than in Ag_3Na_9LTA which can be attributed to the covalent rather than electrostatic interaction of the Ag cations with the O_F, leading to less T-O-T bonds distortion and shifting.[12, 16] These bands are less prounonced in $Na_{12}LTA$ than in Ag_3Na_9LTA, suggesting that the distortion and the energy shift mainly due to interaction of the AgCLs with O_F (Figure 3B, column III) which do not exist in the parent $Na_{12}LTA$. Thus, the significantly distorted and shifted bands

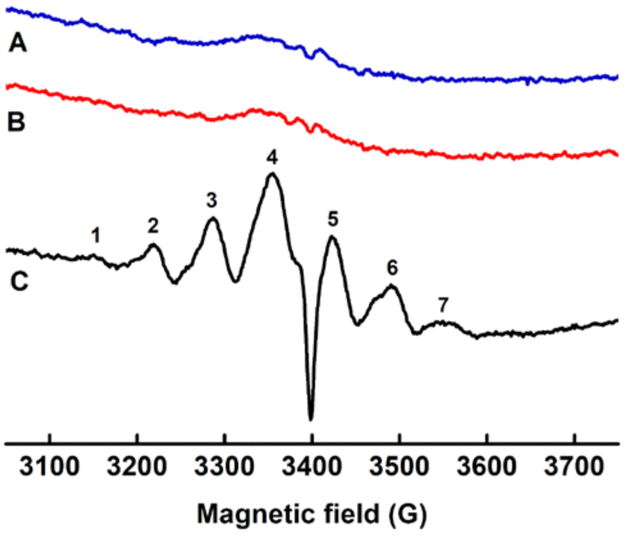

Figure S6. ESR spectra of the sample in (A) hydrated (B) dehydrated (C) dehydrated followed by H_2 reduced state. H_2 reduction performed on dehydrated sample at room temperature that exposed with a mixture of 5% H_2 in N_2 gas during 90 min with the total gas flow rate of 50ml/min.

in Ag_3Na_9LTA compared to Na_{12} and $Ag_{12}LTA$, could arise from the presence of both Na/Ag cations and AgCLs perturbed T-O-T bonds. Since all the LTA framework vibrations (S6Rs, S4Rs, D4Rs and lattice) are part of the T-O-T vibrations and not separate into different vibrational modes, it is however difficult to unambiguously identify the exact location and interaction at the origin of the perturbation.[20] Overall, FTIR shows that a strong interaction between extra-framework AgCLs, Na, and Ag cations and the framework oxygen (O_F) is reversibly building up and decreasing upon dehydration and rehydration respectively in line with the results of the EXAFS analysis.

ESR Analysis

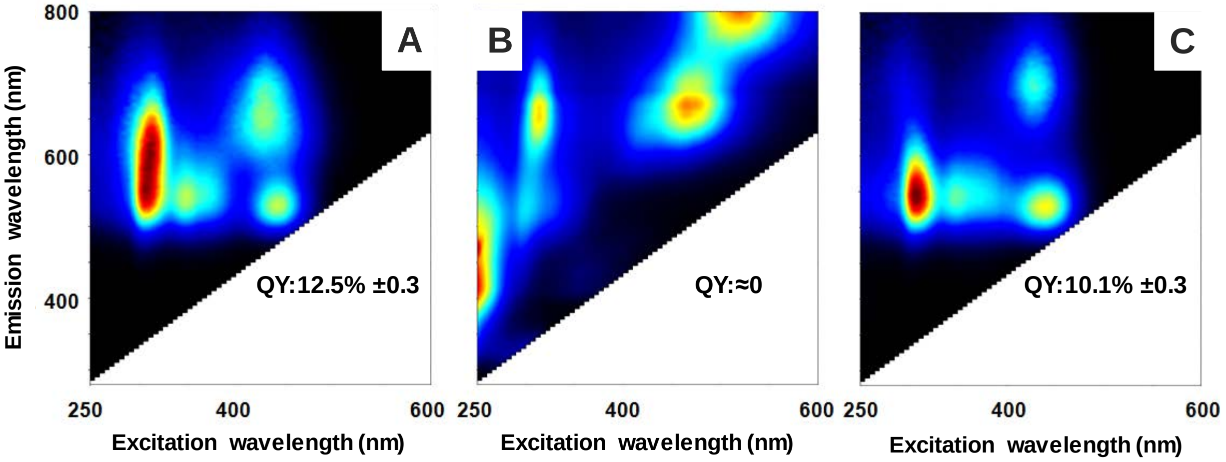

Figure S7. 2D excitation-emission plots of Ag_3K_9LTA sample in A) Hydrated, B) Dehydrated, and C) Rehydrated states. The insets show the QY % of the samples at the maximum excitation of 310 nm.

References

1. K. Beck, H. Pfeifer and B. Staudte, *Microporous Mater.*, 1993, 2, 1-6.
2. Y. Kim and K. Seff, *J Phys Chem* 1987, 91, 671-674.
3. L. R. Gellens, W. J. Mortier, R. A. Schoonheydt and J. B. Uytterhoeven, *J Phys Chem* 1981, 85, 2783-2788.
4. K. Yang and K. Seff, *J Am Chem Soc*, 1978, 100, 6989-6997.
5. Y. Suzuki, T. Miyanaga, H. Hoshino, N. Matsumoto and T. Ainai, *Phys Scr*, 2005, 115, 765-768.
6. T. Miyanaga, H. Hoshino and H. Endo, *J. Synchrotron Rad.*, 2001, 8, 557-559.
7. T. Sun and K. Seff, *Chem. Soc. Rev.*, 1994, 94, 857–870.
8. T. Wąsowicz and J. Michalik, *Int J Rad Appl Instrum* 1991, 37, 427–432.
9. A. Mikula, M. Krol and A. Kolezynski, *J Mol Model*, 2015, 21, 275.
10. M. Krol, W. Mozgawa, W. Jastrzebski and K. Barczyk, *Micropor Mesopor Mat*, 2012, 156, 181-188.
11. W. Mozgawa, W. Jastrzebski and M. Handke, *J Mol Struct*, 2005, 744, 663-670.
12. B. B. Iversen, S. Latturner and G. Stucky, *Chem. Mater.*, 1999, 11, 2912-2918.

13. J. E. Sponer, Z. Sobalik, J. Leszczynski and B. Wichterlova, *J Phys Chem B*, 2001, 105, 8285-8290.
14. S. E. Latturner, J. Sachleben, B. B. Iversen, J. Hanson and G. D. Stucky, *J Phys Chem B*, 1999, 103, 7135-7144.
15. J. H. Kwaka, T. Vargab, C. H. F. Pedenc, F. Gaoc, J. C. Hansond and J. Szany, *J Catal*, 2014, 314, 83-93.
16. T. Carey, C. C. Tang, J. A. Hriljac and P. A. Anderson, *Chem Mater*, 2014, 26, 1561-1566.
17. E. Broclawik, J. Datka, B. Gil and P. Kozyra, *Phys Chem Chem Phys*, 2000, 2, 401-405.
18. Z. Sobalik, J. Dedecek, I. Ikonnikov and B. Wichterlova, *Micropor Mesopor Mat*, 1998, 21, 525-532.
19. O. Fenwick, E. Coutino-Gonzalez, D. Grandjean, W. Baekelant, F. Richard, S. Bonacchi, D. De Vos, P. Lievens, M. Roeffaers, J. Hofkens and P. Samori, *Nat Mater*, 2016, 15, 1017-1022.
20. J. A. Creighton, H. W. Deckman and J. M. Newsam, *J Phys Chem*, 1994, 98, 448-459.